CHAPTER - VII

(PHOTO) ELECTROCHEMICAL CHARACTERIZATION OF ANTIMONY CHALCOGENIDE THIN FILMS

7.1 INTRODUCTION

Semiconductor liquid junction solar cells have been attracting attention in the last few years due to growing interest in solar energy conversion [1-5]. These cells are simple in construction and have the advantage that they can be used for both photovoltage and chemical energy conversion.

Antimony trisulphide is a *n*- type semiconductor which has received a little attention as a potential candidate in solar energy conversion [6-11]. Light to electrical energy conversion efficiency (η) of 3.9 % for chemically deposited annealed Sb_2S_3 films with silicotungstic acid has been reported by Savadogo and Mandal [6]. Others [7-10] reported the efficiency of photoelectrochemical (PEC) cell formed with chemical bath deposited Sb_2S_3 thin films less than 0.01 %. Relatively smaller efficiency for the cell than that of expected was due to the high electrical resistivity of photoelectrodic material and strong absorption of incident light in the electrolyte [10]. PEC studies on spray deposited Sb_2S_3 thin films from *non* -aqueous medium have already been reported by Killedar et al. [11]. The fill factor and power conversion efficiency of the cell was 0.34 and 0.058 % respectively. The basic requirements of a good PEC cells are thin film photoelectrodes of low resistivity and large grain size [12]. The large grain size leads to reduction of grain boundary area of thin films with important consequences for efficient energy conversion. The low resistivity of the photoelectrode minimizes the series resistance of the PEC cell.

Photoconducting antimony trisulphide thin films are generally prepared by vacuum evaporation or by sintering technique using powdered Sb_2S_3 compound as the starting material. This creates the difficulty of achieving the stoichiometric films due to wide differences of the vapour pressures of the constituents at the deposition temperature. Recently there has arisen a sustained effort to produce different chalcogenide thin films for PEC solar cells applications by simple and inexpensive spray pyrolysis technique [13-15]. Preparation and characterization of Sb_2S_3 thin films by spray pyrolysis using *non* -aqueous solvent has already been published elsewhere [16-17]. The present chapter reports on the PEC characterisation of antimony chalcogenide thin films based PEC solar cells such as I-V in dark and light, photoresponse, photovoltaic output, photovoltaic rise and decay, C- V and spectral response characteristics. The effect of substrate on the performance of *n*- Sb_2S_3 / polyiodide PEC solar cells has been discussed and the band edges of Sb_2S_3 have been located.

7.2 EXPERIMENTAL

7.2.1 Construction of photoelectrochemical (PEC) cell

A PEC cell consists of i) a semiconductor photoelectrode , ii) an electrolyte and iii) a counter electrode. Requirements of a photoelectrode, an electrolyte and a counter electrode have been given in [S. Chandra in Photoelectrochemical Solar Cells] [21].

The Sb_2S_3 thin films were prepared by spraying 25 cc solution mixture onto preheated fluorine doped tin oxide coated glass microslides (sheet resistance ≈ 10 Ω/□), Titanium (Ti) and Stainless Steel (S.S.) substrates in separate sets of the experiments. The optimized substrate temperature for deposition of the films on FTO glass was 250 ^oC [16] while it was 175 ^oC for Ti and S.S. substrates. Comparatively lower decomposition temperature for metallic substrates than that of FTO coated glass is due to higher thermal conductivity of former than the latter.

The PEC cell was constructed by using *n*- Sb_2S_3 thin film as photoelectrode , polyiodide an the electrolyte and graphite as the counter electrode. The PEC cell has the configuration

M - *n*- Sb_2S_3 | 0.5M KCl + 0.5M KI + 0.01M I_2 | C

where, M = F: SnO_2, Ti or S.S.

The water lens was interposed between the lamp and the cell to avoid the heating of the cell. The distance between the photoelectrode and counter electrode was 0.2 cm. The photoanode area exposed to light was ≈ 1 cm^2. The area of the semiconducting thin film other than that in contact with electrolyte was covered by epoxy resin (Araldite, India) to annul any contribution due to the base contact oxide material with the electrolyte and its interference in the measured values of the net photocurrent density.

For measurement of power output characteristics, a two-electrode configuration consisting of the thin film photoelectrode and graphite as the

counter electrode was used. Measurements for the power output characteristics, I-V plots and Mott- Schottky plots were made at fixed intervals after waiting for sufficient time to equilibrate the system at that setting. The Mott - Schottky plots were plotted using a LCR bridge (Aplab model 4912) at two different built - in - frequencies of 100 Hz and 1 KHz. The annealing was performed in N_2 for half hour at 200 ^oC. The thin films were etched in 5 % HCl in water.

7.3 (PHOTO)ELECTROCHEMICAL CHARACTERIZATION OF ANTIMONY CHALCOGENIDE BASED PEC CELL

7.3.1. Current-Voltage (I -V) characteristics

The circuit diagram used to study the I-V characteristics of PEC cell in dark and in light is shown in Fig. 7.1. A ten turn potentiometer (10 KΩ) is used to vary the potential applied to the cell. The current through the circuit and voltage applied to the cell are measured by using MICo make MIC-6E digital multimeters. All the voltages are measured with respect to SCE. The cell is illuminated with 500 Watt tungsten filament lamp.

7.3.2 Photoresponse

The photo response of the PEC cell was studied by measuring the short circuit current (I_{sc}) and open circuit voltage (V_{oc}) for different illuminating intensities. The experimental arrangement is depicted in Fig. 7.2 which consist of tungsten filament lamp to irradiate the cell, a water lens and the PEC cell. The intensities at different distances was measured with CEL Suryampi.

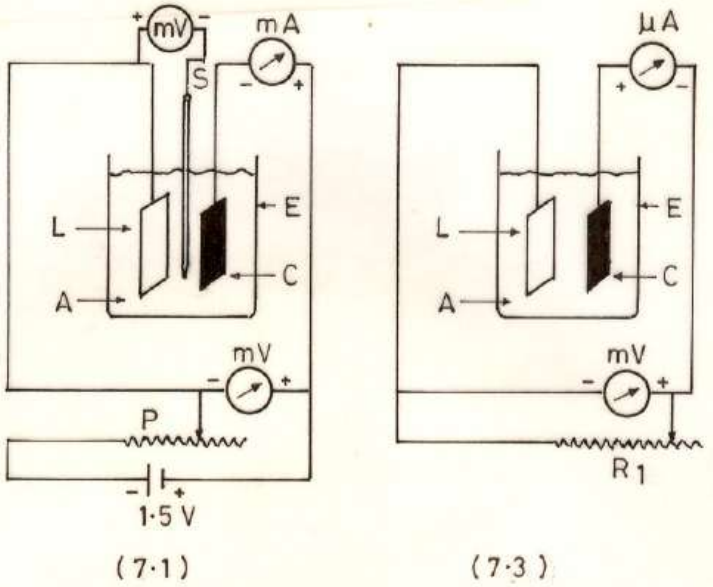

(7·1) (7·3)

E – PEC cell ; C – counter electrode ; A – photoanode ;
P – potentiometer ; L – light ; μA – microammeter ;
mV – millivoltmeter ; S – SCE .

Fig. Experimental circuit diagram for
(7·1) I-V characteristics of PEC cell
(7·3) Photovoltaic output characteristics of PEC cell .

1 – Photoanode
2 – Counter electrode
3 – SCE
4 – Electrolyte

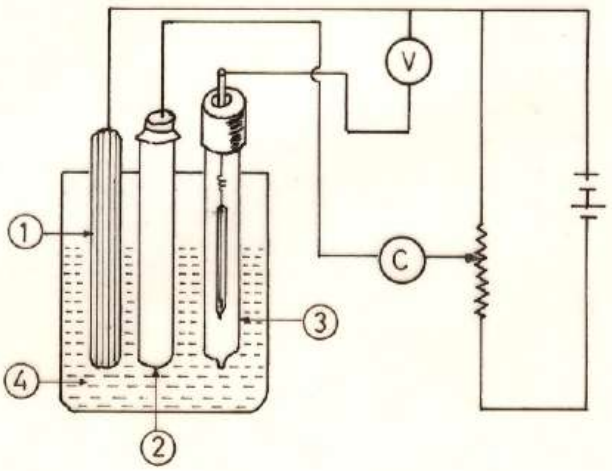

Fig. 7·5 Circuit diagram for capacitance voltage characteristics of the PEC cell .

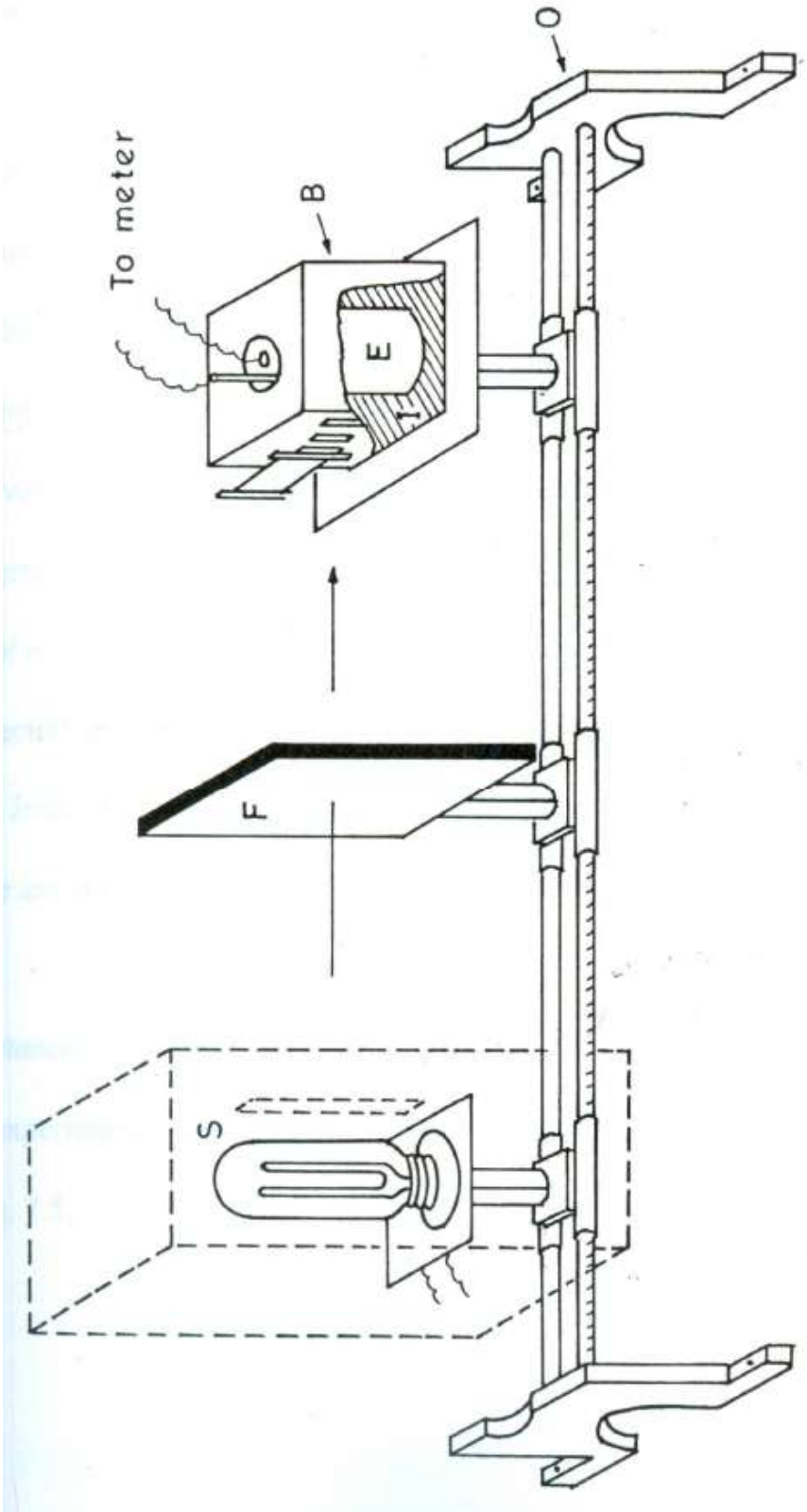

S – Light source ; B – Bakelite box ; E – ECPV cell ;
I – Insulator ; O – Optical bench ; F – Water filter .

Fig. 7:2 - Experimental set-up for dynamic current-voltage characteristic.

7.3.3 Photovoltaic output characteristics

Photovoltaic output characteristic of PEC cell was studied using circuit diagram shown in Fig.7.3. A ten turn potentiometer (10 kΩ) is used as a variable load resistance. The current through the load is measured with MICo make (MIC-6E) microammeter. The output voltage is measured with digital multimeter model MIC-9A.

7.3.4 Transient Photoresponse

Transient Photoresponse of the PEC cell is studied by measuring the open circuit voltage (Voc) as a function of time. Illuminating light is kept ON till the Voc gets saturated then the light is put OFF.

7.3.5 Spectral response

The spectral response of the PEC cell was recorded by a monochromator Spekol (Carl Jena, Germany make) in the wavelength range between 400 nm to 850 nm. The circuit diagram for spectral response measurement is shown in Fig. 7.4.

7.3.6 Capacitance- Voltage (C- V) characteristic in dark

The experimental arrangement to carry out the C- V measurements is shown in Fig. 7.5.

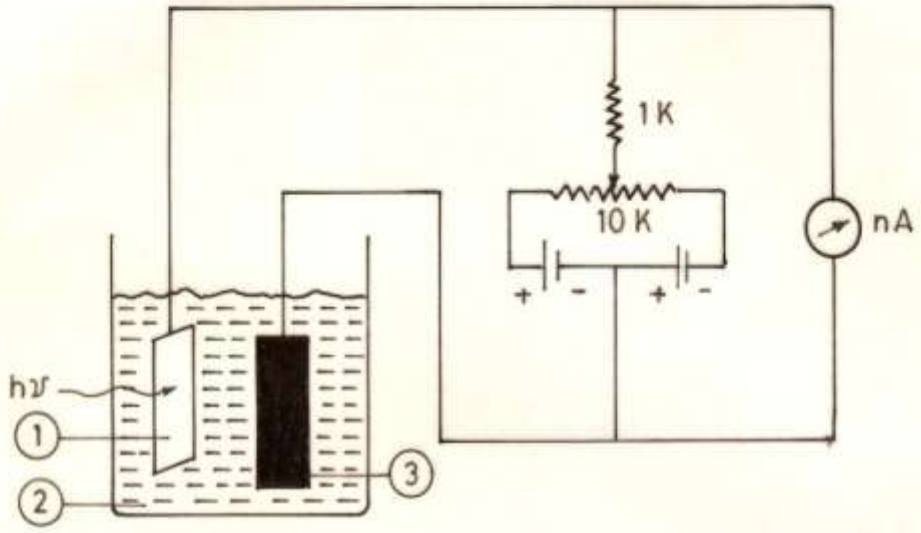

1) Photoelectrode 2) Electrolyte 3) Counter electrode

Fig. 7·4 - Circuit diagram for spectral response measurement of PEC cell.

7.4 RESULTS AND DISCUSSION

Spray deposited antimony chalcogenide (namely Sb_2S_3 and Sb_2Se_3) prepared on FTO coated glass from aqueous and *non* - aqueous media were tested for their photoactivity by using them in PEC cell. The various electrolytes tested were 1M polysulphide (NaOH + Na_2S + S), polyiodide [0.5M (KCl + KI) + 0.01M I_2] and 1M ferri- ferro cyanide [$K_4Fe(CN)_6$/ $K_3Fe(CN)_6$]. It has been found that all the films show photoactivity only in polyiodide electrolyte. Irrespective of preparation medium (aqueous or *non* - aqueous), Sb_2S_3 and Sb_2Se_3 found to have *n*- and p- type of conductivity respectively in PEC cell confirming the results obtained by TEP measurements. Following are the results on open- circuit voltage (Voc) and short- circuit current (Isc) for the films prepared on FTO coated glass substrates.

Film	Isc (μA)	Voc (mV)
A- Sb_2S_3	1	35
NA- Sb_2S_3	800	209
A- Sb_2Se_3 (SDO)	0	2
NA- Sb_2Se_3 (SDO)	0.2	12
A- Sb_2Se_3 (SU)	1.5	10
NA- Sb_2Se_3 (SU)	0	6

A- Aqueous, NA- Non-Aqueous, SDO- Selenium Dioxide, SU- Selenourea

It is seen that only NA- Sb_2S_3 films showed the acceptable performance. Relatively smaller photoresponse for other films is due to slight deviation of

material from the stoichiometry. Further, these films deposited on metallic substrates viz. titanium (Ti) and stainless steel (S.S.) were also tested for their photoactivity in PEC cells. Only the film NA- Sb_2S_3 showed the acceptable photoresponse. This is due to relatively ordered structure, higher grain size and formation of perfect stoichiometry of Sb_2S_3 from *non* - aqueous medium. Therefore only these films (NA- Sb_2S_3) were further PEC characterized in detail for calculation of physical parameters and location of band edges of Sb_2S_3.

The PEC cell with configuration Sb_2S_3 / 0.5M (KCl + KI) + 0.01M I_2 / C was formed in order to check the conductivity type exhibited by Sb_2S_3 thin films. It is seen that even in dark PEC cell gives some dark voltage V_d with Sb_2S_3 thin film as a negative electrode and graphite electrode as positive. The origin of this voltage is attributed to the difference between two half cell potentials in the PEC cell. After illumination of the junction, the magnitude of the open circuit voltage increases with negative polarity towards the Sb_2S_3 thin film. Thus the cathodic behavior of photovoltage of the semiconductor is observed which indicates that the Sb_2S_3 thin films are of *n*- type [7-11].

7.4.1 I- V characteristics

I- V characteristics of the PEC cell formed with *n*- Sb_2S_3 thin film electrode in dark and under light illumination of 80 mW/cm^2 are shown in Fig. 7.6. The *non* - symmetric nature of the I-V curve in forward and reverse bias shows the rectification property of semiconductor electrolyte junction. After illumination, shifting of the I-V curve in the fourth quadrant reveals that the

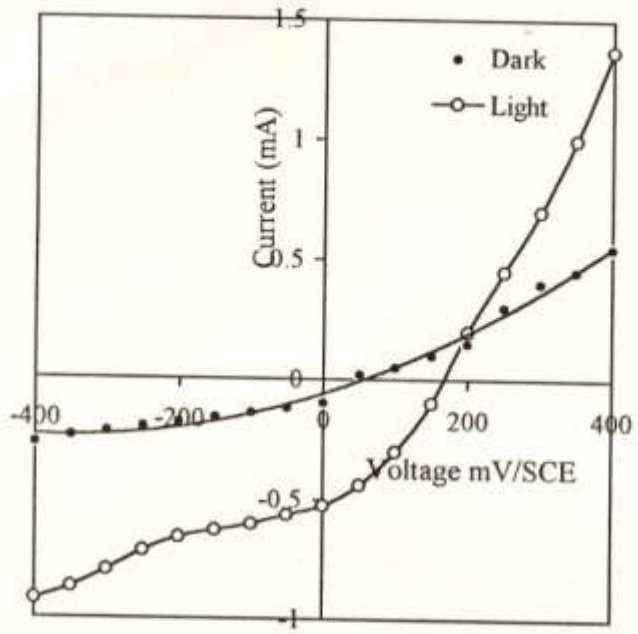

Fig. 7.6 : I- V characteristics of *n* - Sb_2S_3/ 0.5 M (KCl+ KI) + 0.01 M I_2 / C PEC cell in dark and in light

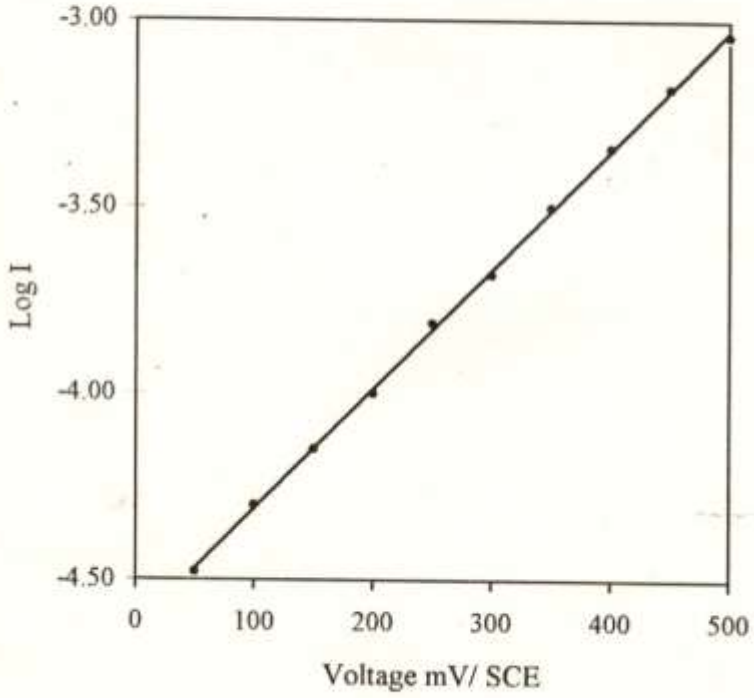

Fig. 7.7 : Log I versus voltage plot for n-Sb_2S_3/ polyiodide PEC solar cell in dark.

cell can work as a generator of electricity. I- V curve in third quadrant is not influenced much by applied reverse bias, but a large photocurrent flows in the first quadrant. The information of the junction parameter can be obtained using a simple diode equation as

$$V = \frac{nKT}{e} \ln\left(\frac{I}{Io} + 1\right) \qquad (7.1)$$

where n is the junction quality factor, I_o , the reverse saturation current, V, the forward bias voltage and I, the forward current in dark. Under illumination, V and I are replaced by V_L and I_L respectively in equation (7.1). The plot of Log I against V in dark (Fig. 7.7) shows linear behavior with dark junction ideality factor 'n_d' to be 2.11. The higher value of n_d is indicative of the series resistance effect and recombination mechanism at the semiconductor-electrolyte interface [18]. However the current in the reverse bias does not saturate. In PEC cell this behavior is due to following reasons [19] : (i) The effective barrier height decreases because of the interfacial layer (ii) Electron-hole pairs are thermally generated in the depletion layer under the condition of large reverse bias and (iii) The current increases due to the onset of the electron injection from an electrolyte because barrier height become thin enough for tunneling to take place.

7.4.2 Photoresponse characteristics

The short circuit current and open circuit voltage (I_{sc} and V_{oc} respectively) are measured as a function of light intensity F_L for the cell and a result is shown in Fig. 7.8. I_{sc} shows linear variation with light excitation level which can be explained by the relation [19]

$$I_{sc} = C\, F_L$$

where C is proportanility constant The plot of V_{oc} against log F_L is shown in Fig. 7.9 which is linear and is represented by the relation [19]

$$V_{oc} = \frac{nKT}{e} \ln F_L + \text{Constant} \qquad (7.2)$$

The slope of the graph gives the junction ideality factor n_l to be 1.34 which is less than that of n_d. These results are in consonance with those reported earlier [20-21].

7.4.3 Photovoltaic output characteristics

Typical photocurrent density versus photovoltage characteristics (Power output characteristics) of *n*- Sb_2S_3 films on various substrates / polyiodide under illumination is shown in Figs. 7.10 to 7.12. The efficiency η (in %) was calculated from the relation

$$\eta = \frac{V_{oc}\, I_{sc}\, FF}{P_{input}} \times 100 \qquad (7.3)$$

where P_{input} is input light energy. Fill factor (ff) was calculated from the relation

$$ff = \frac{Im\ Vm}{Isc\ Voc} \qquad (7.4)$$

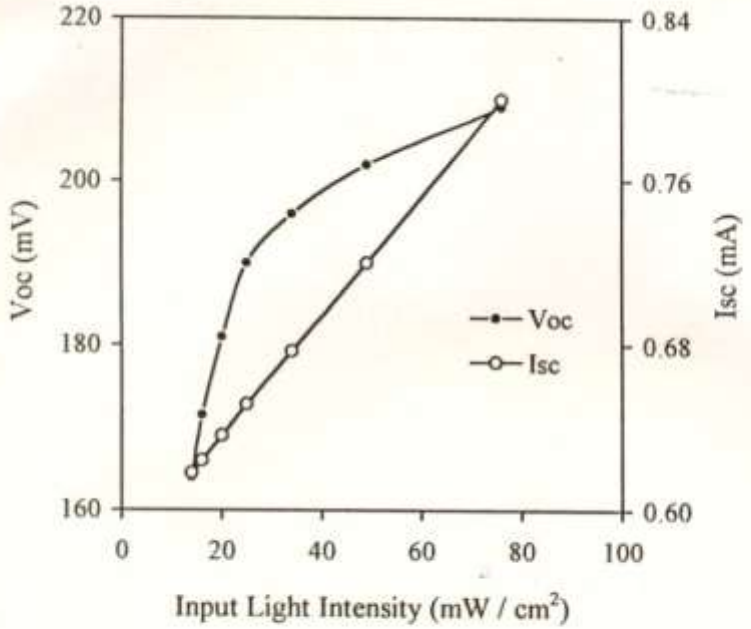

Fig. 7.8 : Variation of Isc and Voc with light intensity FL for *n* - Sb_2S_3 / 0.5 M (KCl + KI) + 0.01 M I_2 / C PEC solar cell

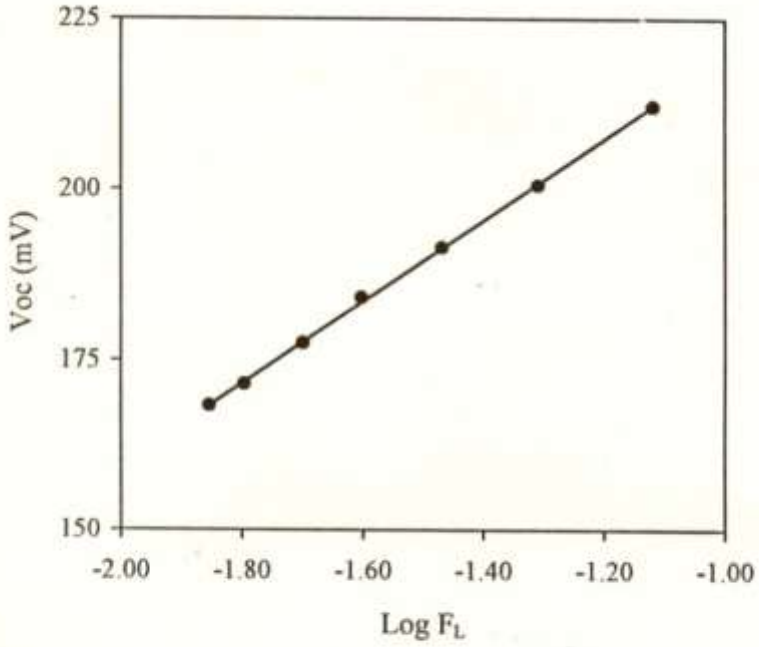

Fig. 7.9 : Plot of Voc versus Log FL for *n* - Sb_2S_3 / 0.5 M (KCl + KI) + 0.01 M I_2 / C PEC solar cell

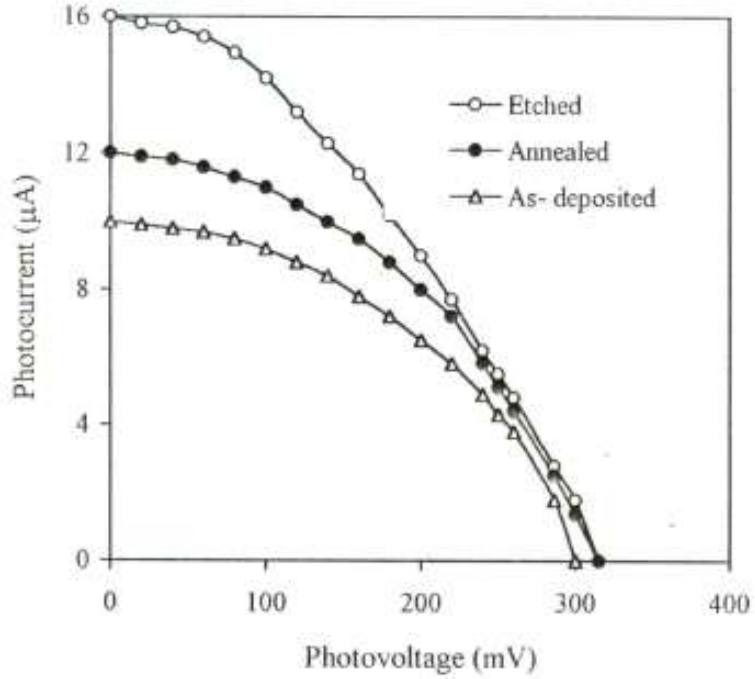

Fig. 7.10 : Plot of power output characteristics for n-Sb_2S_3 (on Ti) / 0.5 M (KI+KCl) + 0.01 M I_2 / C PEC cell

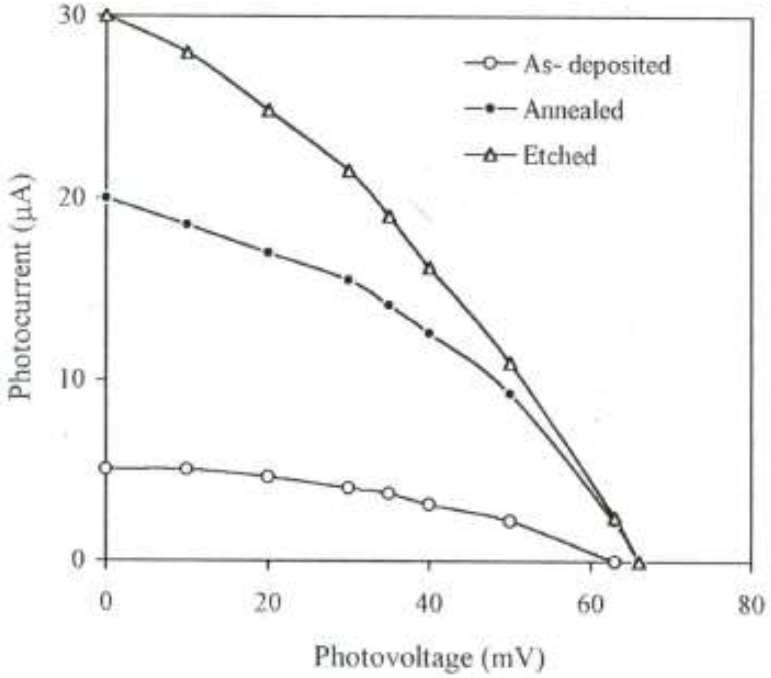

Fig. 7.11 : Plot of power output characteristics for *n* - Sb_2S_3 (on Stainless steel) / 0.5 M (KI+KCl) + 0.01 M I_2 / C PEC cell

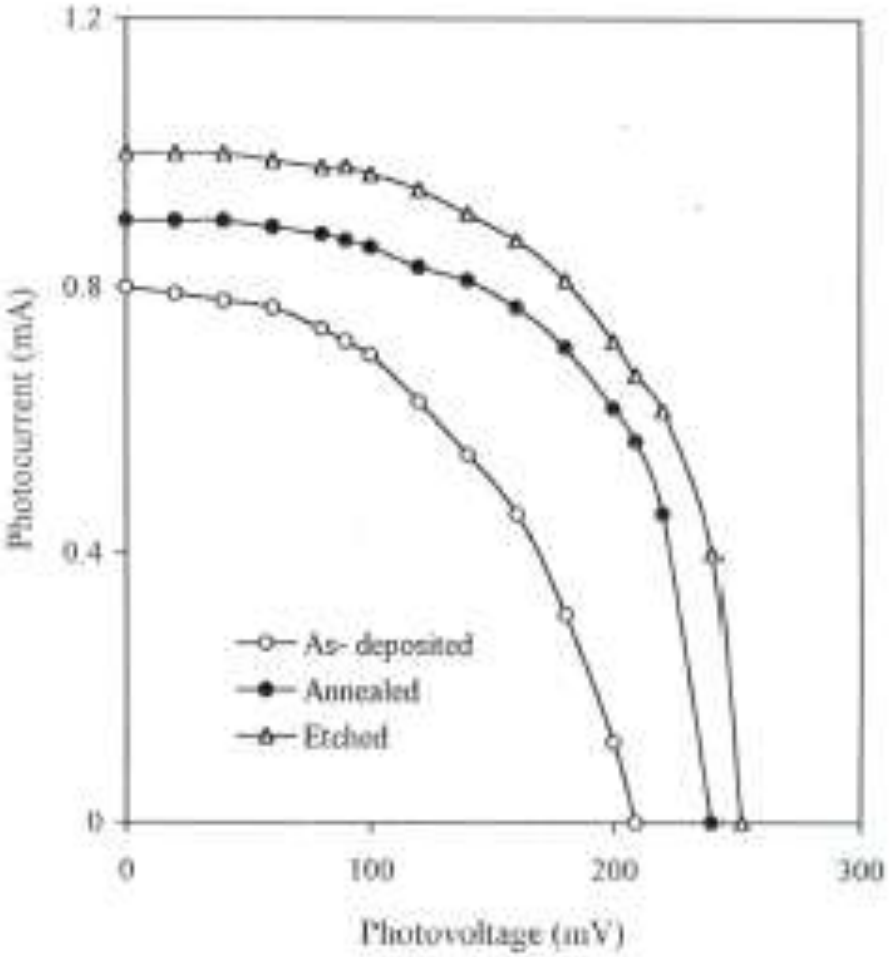

Fig. 7.12 : Plot of power output characteristics for n-Sb_2S_3 (on FTO coated glass) / 0.5 M (KCl-KI) + 0.01 M I_2 / C PEC cell

Series resistance R_s and shunt resistance R_{sh} were estimated from slope of

$$\left(\frac{dI}{dV}\right)_{V=0} \cong \left(\frac{1}{R_{sh}}\right) \tag{7.6}$$

power output characteristics using the relation [22]

$$\left(\frac{dI}{dV}\right)_{I=0} \cong \left(\frac{1}{R_s}\right) \tag{7.5}$$

Important parameters that are obtained from the power output plots are tabulated in Table 1.

It is seen that the shunt resistance changes favorably on surface treatments. For etched films, it is 333 K, 40 K and 7.33 K Ω for the films on titanium (Ti), stainless steel (S.S.) and FTO coated glass respectively. R_{sh} in case of the thin film polycrystalline solar cell mainly arises due to columnar grains with lengths close to the thickness of thin film itself. For thin films with low packing density of grains, there is a likelihood of easy leakage paths through the grain boundaries. The process of annealing increases the packing density and strong adhesion to the substrate. Etching process contribute to the increase in the junction area so that an increase in the shunt resistance is observed [23].

It is seen that the series resistance R_s also changes favorably to better values on surface treatments. On etching the films on Ti, S.S. and FTO it is 4.8 K, 0.700 K and 3.8 Ω respectively. The contribution to R_s comes from bulk

Table 1 Power output parameters using Sb_2S_3 films on various substrates/ polyiodide PEC solar cells at different conditions.

Condition of film	Isc ($\mu A/cm^2$)	Voc (mV)	η (%)	ff (%)	R_s (Ω)	R_{sh} ($K\Omega$)
Titanium (Ti) substrate						
As-deposited	10	300	0.0025	41.20	20012	150
Annealed	12	315	0.0037	42.32	13333	250
Etched	16	315	0.0047	47.14	4871	333
Stainless Steel (S.S.) substrate						
As-deposited	5	63	0.0004	41.42	2732	25
Annealed	20	66	0.0011	41.66	1615	30
Etched	30	66	0.0020	50.50	714	40
FTO coated glass substrate						
As-deposited	800	209	0.154	46.05	68.75	4.40
Annealed	931	240	0.248	57.4	6.08	6.28
Etched	1006	251	0.298	59.5	3.80	7.33

resistance of the film, the contacts to the thin film and the external circuit. Also the deposition temperatures for the films on the metallic and FTO coated glass

substrates are different which may lead to the different reaction mechanisms during film formation. The smaller value of Rs for the film deposited on FTO coated glass may be due to formation of good quality films due to suitable substrate temperature.

The calculated efficiency is about 0.0004 % for the S.S. substrate PEC cell. For the Ti and FTO glass substrate PEC cells the power output plot shows a remarkable improvement in efficiency of 0.0025 % and 0.15 % respectively. On annealing the films on FTO glass substrate, the efficiency increases from 0.15 to 0.24 % and etching the films it increases from 0.24 to 0.29 %. This can attributed to the low series resistance ($R_s \approx 3.8\ \Omega$) and high shunt resistance ($R_{sh} \approx 7.33\ K\Omega$) of the FTO coated glass substrate based PEC solar cell compared to the S.S. and Ti substrate based PEC solar cells. Inspite of high R_{sh} for metallic substrate based PEC cell their R_s is also large (~ KΩ) which results in lower efficiency of the PEC cell.

7.4.4 Transient photoresponse

The photovoltage rise and decay (Fig. 7.13) curve reveals that increase in photovoltage is almost instantaneous. The plot of log V_{oc} against log t (Fig. 7.14) is linear obeying the relation [24-25]

$$V_{oc}(t) = V_{oc}(o)\ t^{-b} \qquad (7.7)$$

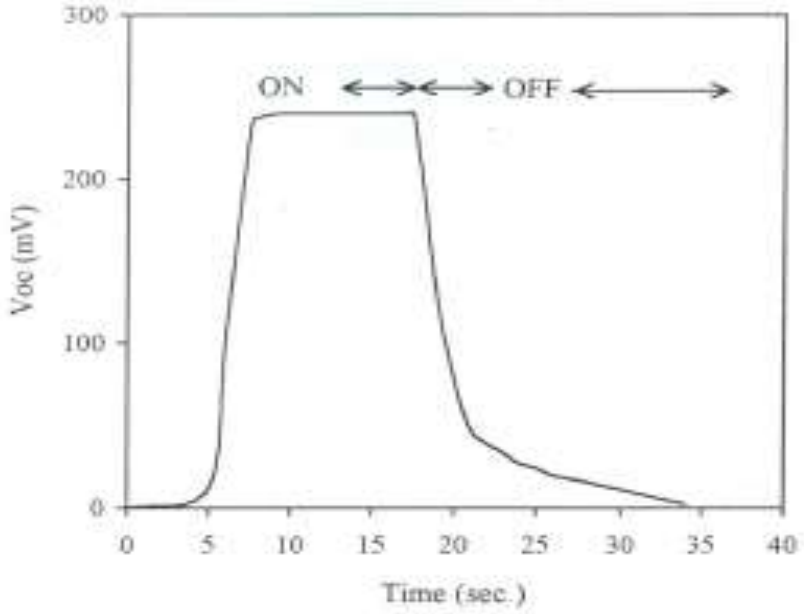

Fig. 7.13 : Photovoltaic rise and decay curve for *n* - Sb_2S_3 / 0.5 M (KCl + KI) + 0.01 M I_2 / C PEC solar cell

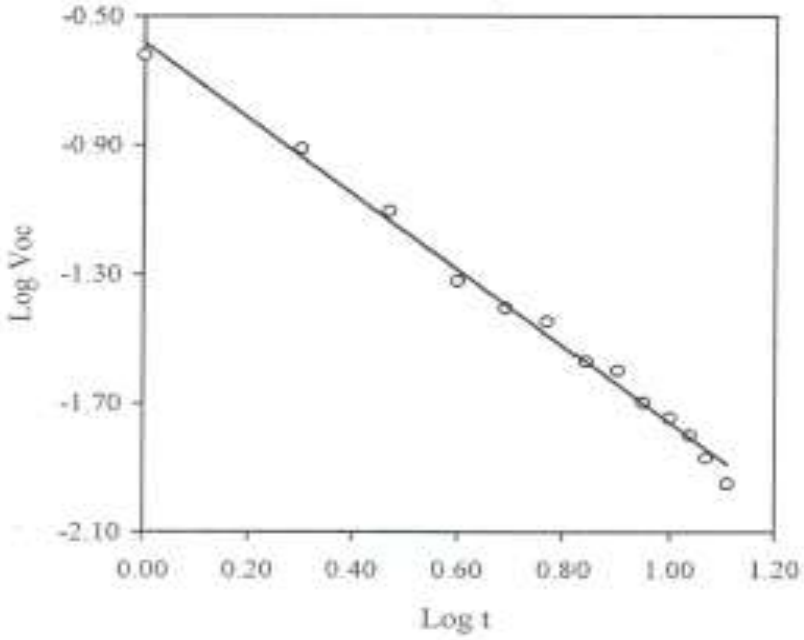

Fig. 7.14 : Plot of Log Voc versus Log t for Photovoltaic decay curve

where $V_{oc}(o)$ and $V_{oc}(t)$ are open circuit voltages at t=0 and t seconds respectively and b, the decay constant. The linearity of the plot suggests that the kinetics involved in voltage decay process is of second order [25]. The decay constant, calculated from the slope of the graph , is found to be 1.18.

7.4.5 Spectral response studies

Spectral response studies were conducted for Sb_2S_3 thin film electrode (on FTO coated glass)/ polyiodide / C PEC system by plotting the short circuit photocurrent density (I_{sc}) as a function of wavelength. Variation of I_{sc}, absorbance due to the Sb_2S_3 film and absorbance due to the polyiodide electrolyte has been shown in Fig. 7.15. It is seen that at the onset of photon energy, at the edge of the band gap there is a sharp rise in the photocurrent density, attaining maximum. The lower photocurrent on the shorter wavelength side is due to the strong absorption of light in the electrolyte (below 675 nm) and the larger amount of surface recombination of the photogenerated minority carriers. The quantum efficiency, Q_F is given by [4]

$$Q_F = \frac{\text{Number of photoelectrons generated / area}}{\text{Number of incident photons / area}} \qquad (7.8)$$

and is calculated from the equation

$$Q_F = \frac{I_{SC}\ (A/\ cm^2)\ X\ h\nu\ (eV)}{q\ X\ \text{Intensity of light}\ (W / cm^2)} \qquad (7.9)$$

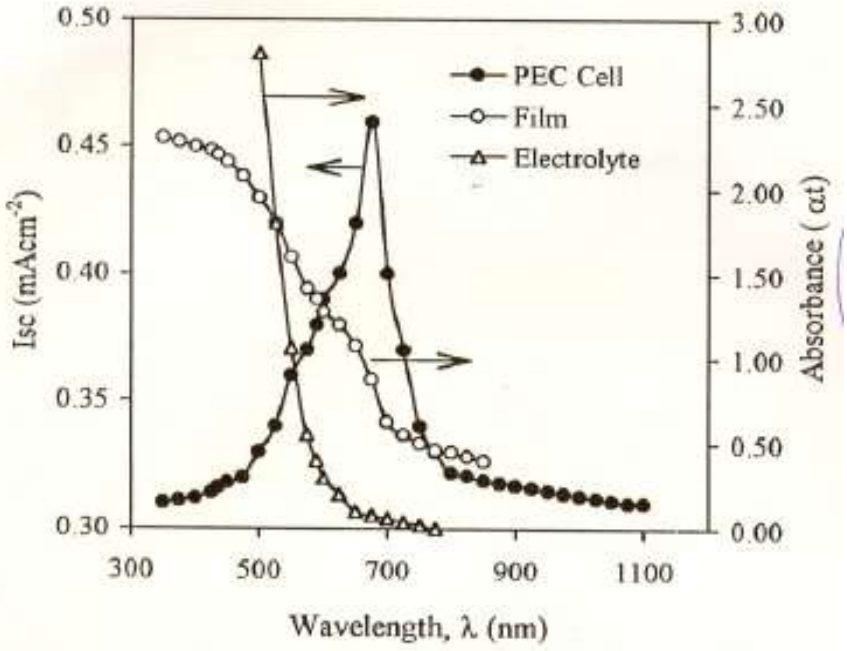

Fig. 7.15 : Variation of short circuit current density, absorbance due to film and absorbance due to electrolyte as a function of wavelength for Sb_2S_3/ Polyiodide PEC solar cells.

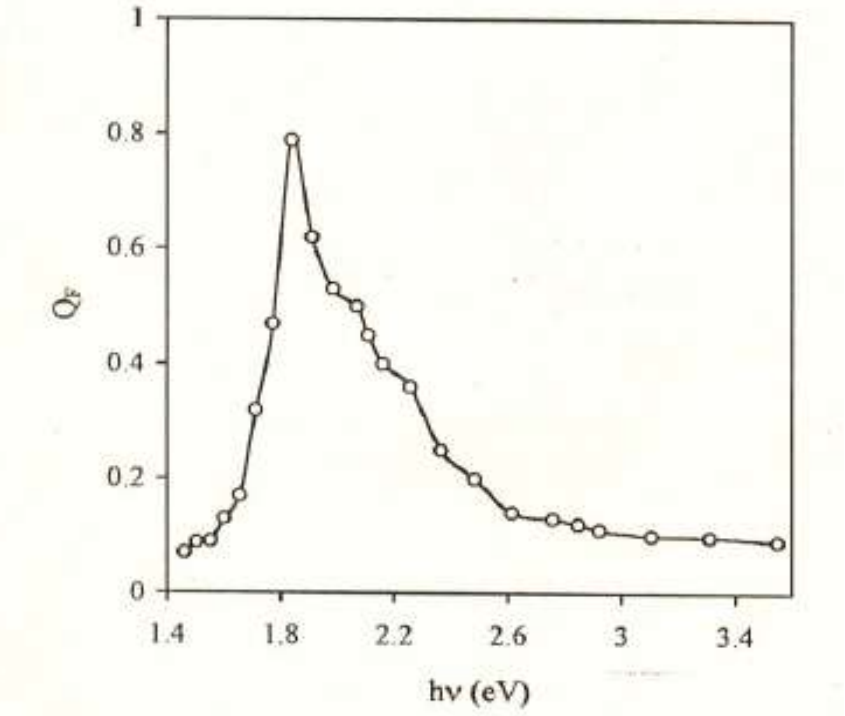

Fig. 7.16 : A plot of quantum efficiency as a function of photon energy for n- Sb_2S_3 / polyiodide PEC solar cell

As per Butler [26]

$$Q_F = \left\{ 1 - \frac{e^{-\alpha W}}{1 + \alpha L_P} \right\} \qquad (7.10)$$

where α the absorption coefficient, L_P the hole diffusion length, q the electronic charge and W the width of the depletion layer. A plot of quantum efficiency as a function of photon energy in Fig. 7.16 indicates that the etched phoelectrode yields a maximum yield of 79 %.

In the vicinity of the absorption edge, such that $\alpha L_P << 1$ and $\alpha W << 1$, expanding equation (7.9) and neglecting higher powers of the series expansion of $\exp(-\alpha W)$, we get

$$Q_F = \alpha (W + L_P) \qquad (7.11)$$

For an allowed direct band gap electronic transitions, the absorption coefficient α, near the absorption edge, is given by [27]

$$\alpha = A (h\nu - Eg)^{1/2} / h\nu \qquad (7.12)$$

where A is constant, h the Plank's constant, ν the frequency of incident light.

Substituting the expression for α from equation (7.12) in equation (7.11), we get

$$Q_F = [A (h\nu - Eg)^{1/2} (W + L_P)] / h\nu \qquad (7.13)$$

Therefore,

$$(Q_F h\nu)^2 = A^2 (h\nu - Eg) (W + L_P)^2 \qquad (7.14)$$

The experimental plot of $(Q_F h\nu)^2$ vs. $h\nu$ is linear as shown in Fig. 7.17 as has been expected from the equation (7.14). The intercept on energy axis gives the band gap energy Eg = 1.73 eV. This value is slightly less than the value obtained from optical absorption measurements [16-17] using equation (7.12).

In the region of weak absorption, such that $L_P << 1$ and $\alpha W << 1$ [28] the following relation is valid

$$Q_F = \alpha L_P \tag{7.15}$$

Hence

$$(Q_F)^{-1} = (\alpha L_P)^{-1} \tag{7.16}$$

From the plot of $(Q_F)^{-1}$ vs. $(\alpha)^{-1}$ (Figure 7.18), L_P is obtained from the inverse of the slope and is found to be 0.033 μm. This quantity appears reasonable although as yet there are no independent measurements of this quantity.

7.4.6 Capacitance- Voltage (C- V) characteristics in dark

Figs. 7.19 to 7.21 show the Mott- Schottky (M-S) plots of the *n*- Sb_2S_3 (etched) / polyiodide electrolyte system in dark for Ti, S.S. and FTO coated glass substrates based PEC cells respectively. The value of the flat - band potential, V_{fb}, was obtained at $1/Cs^2 = 0$ on the potential axis according to well- known Mott-Schottky relation [29,30].

$$(1/Cs^2) = (2/ \varepsilon_O \varepsilon_S q N_D) [V- V_{fb} - (kT/q)] \tag{7.17}$$

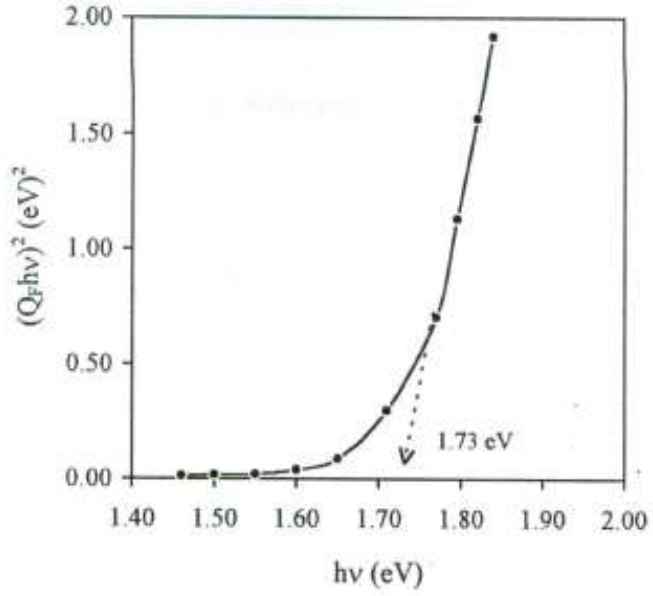

Fig. 7.17 : A plot of $(Q_F h\nu)^2$ as a function of photon energy for n- Sb_2S_3 / polyiodide PEC solar cells

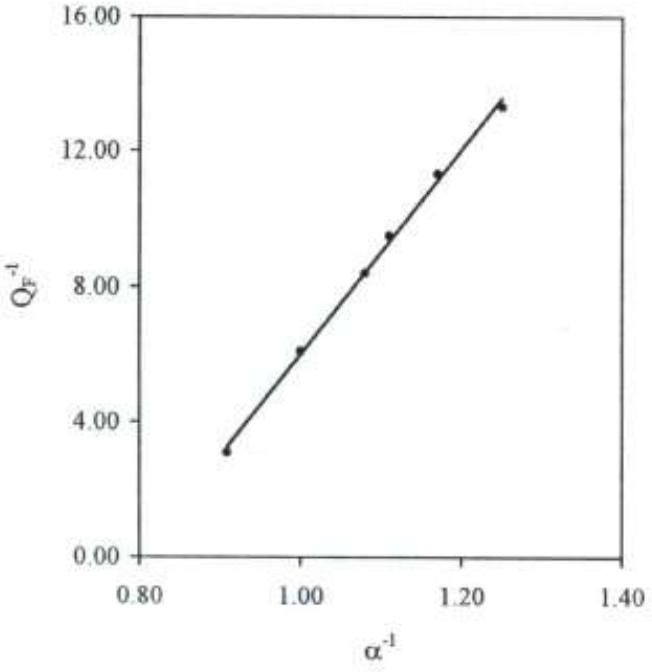

Fig. 7.18 : Plot of Q_F^{-1} versus α^{-1} foe Sb_2S_3 thin film

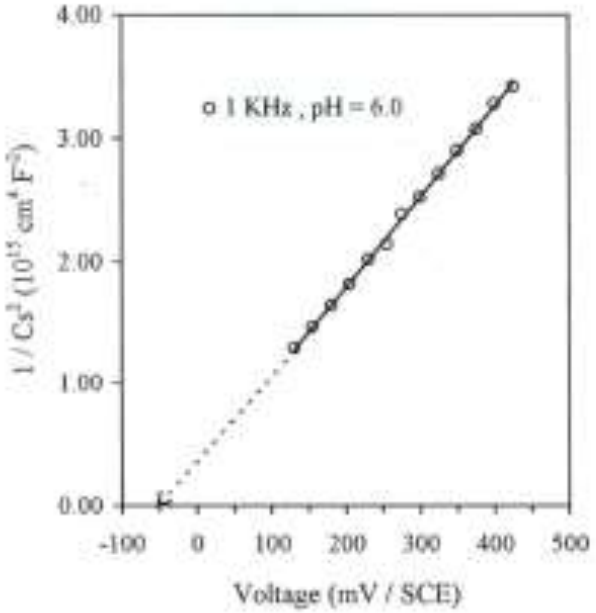

Fig. 7.19 : Mott Schottky plots for Ti /*n* - Sb_2S_3 / 0.5 M (KI+KCl) + 0.01 M I_2 / C PEC solar cell at pH = 6.0 and f = 1 KHz

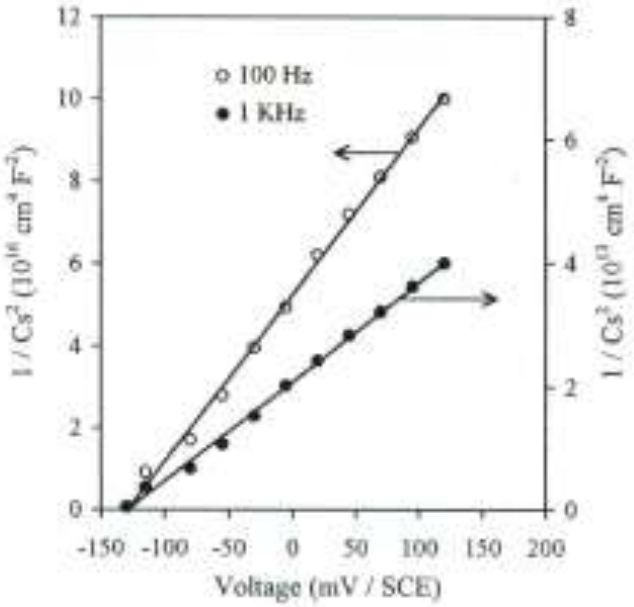

Fig. 7.20 : Mott Schottky plots for SS / *n* - Sb_2S_3 / 0.5 M (KI+KCl) + 0.01 M I_2 / C PEC solar cell at various frequencies

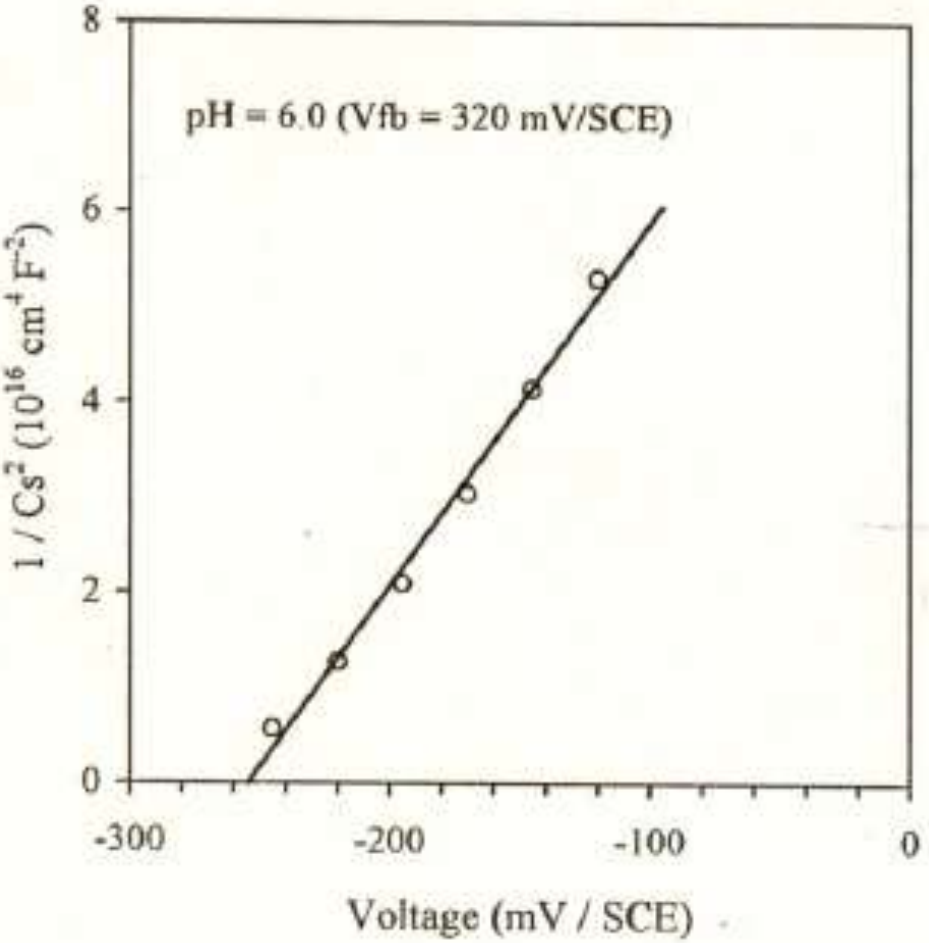

Fig. 7.21 : Mott Schottky plots for FTO / *n* - Sb_2S_3 / 0.5M (KCl + KI) + 0.01M I_2 / C PEC solar cell at Frequency 1 KHz

where Cs is the space - charge capacitance, V_{fb} is the flat band potential, ε_O is the permittivity of free space, ε_S is the static permittivity of the semiconductor; 180 for Sb_2S_3 [31] and N_D is the donor concentration. It is seen that V_{fb} for FTO coated - glass substrate based PEC cell it is relatively higher than that of Ti and S.S. based cells. This is an indication of the fact that there is a likelihood of smaller density of interface states in FTO - glass substrates based systems than that of metallic substrates based PEC cells. Thus, the deviation from the Mott- Schottky plot could be due to the presence of *non* - homogeneous doping levels and surface states in three systems [32].

7.4.6.1 Frequency dispersion of Mott - Schottky plots.

Fig. 7.20 shows the M-S plots drawn for the etched Sb_2S_3 film on S.S. substrate for PEC characterization. It is seen that there is a dispersion in the M-S plots. The slope of the plots increases with increasing frequency from 100 Hz to 1 KHz. It is seen that the plots converge at a single point on the x- axis as observed by other workers [12,33].

Contribution to frequency dispersion can be due to the bulk property of the space - charge layer and occurrence of most of the applied voltage over the Helmholtz layer [34]. If can also be due to [33]:

a) A small contribution from the bulk of the electrode, back ohmic contact, and impedance during the measurements,

b) irregular surface of the film leading to uneven distribution of the modulated input ac signal

c) small contribution of surface states to capacitance [34] ;

d) *non* -uniform distribution of donor species in the region close to the surface of the semiconductor.

The frequency dispersion in the M-S plots will be minimum for those systems where the surfaces are absolutely smooth so that the area of the electrolyte in contact with the semiconductor surface is almost the same. In reality , on the microscopic scale, thin films prepared by spray pyrolysis are always rough, leading to dispersion in M-S plots of the PEC cells.

7.4.6.2 Evaluation of parameters from Mott- Schottky plots and band edge location

The important parameters concerning the photoelectrode were evaluated from the C-V plots at pH ~ 6.0 as described below.

A plots of $1/C_S^2$ versus applied voltage V (Figs. 7.19 to 7.21) give the flat band potentials (V_{fb}) from the intercepts on the voltage axis at $1/C_S^2 = 0$. The $1/C_S^2$ value decreases as V shifts in the negative direction. From the slope of $1/C_S^2$ Vs. V plots, the values of donor densities (N_D) were calculated for each case.

For spray deposited *n*- Sb_2S_3 thin film on Ti substrates, donor density obtained from Mott- Schottky plot is found to be 1.09 x 10^{12} cm^{-3}. And the density of states in conduction band as calculated by the relation [21, 35]

$$Nc = (2/h^3)(2\pi m_e^* kT)^{3/2} \qquad (7.18)$$

comes out to be 1.17 x 10^{18} cm^{-3}.

Now the Fermi level of the semiconductor is related to the donor density (N_D) and the density of states in the conduction band (N_C) by the relation :

$$N_D = N_C \exp [- (E_C - E_F) / kT] \quad (7.19)$$

so that

$$E_C - E_F = - kT \ln (N_D / N_C) = 0.359 \text{ eV} \quad (7.20)$$

This means that the Fermi level (E_F) of Sb_2S_3 is situated 0.359 V below the conduction band edge (in electrochemical scale of energy). But the Fermi level of semiconductor when the energy bands are flat , corresponds to the flat - band potential V_{fb} [21, 35] which is measured to be -0.050 V (SCE) for the films on Ti substrates by Mott-Schottky plot. Thus, with E_F = -0.050 V (SEC), the conduction-band edge is located 0.359 V above the Fermi level , i.e.

Ec = - 0.40 V (SCE).

Band gap of spray deposited Sb_2S_3 as measurement from optical absorption spectrum studies , is found 1.8 eV [16,17]. This implies that the valence band edge is situated 1.8 V below the conduction band edge (in electrochemical scale of energy); i.e. Ev = + 1.4 V (SCE). In the similar way various parameters and band - edge locations for Sb_2S_3 films on S.S. and FTO coated glass substrates were calculated. The energy band diagram for Sb_2S_3 (on Ti) thus obtained is shown in Fig. 7.22 (a).

Now, the amount of equilibrium band bending (V_{bb}) at the semiconductor / electrolyte interface is obtained by the difference of the redox fermi potential ($V_{f,redox}$) of the electrolyte , and the flat band potential (V_{fb}) of the semiconductor in that electrolyte [21, 35] ; i.e.,

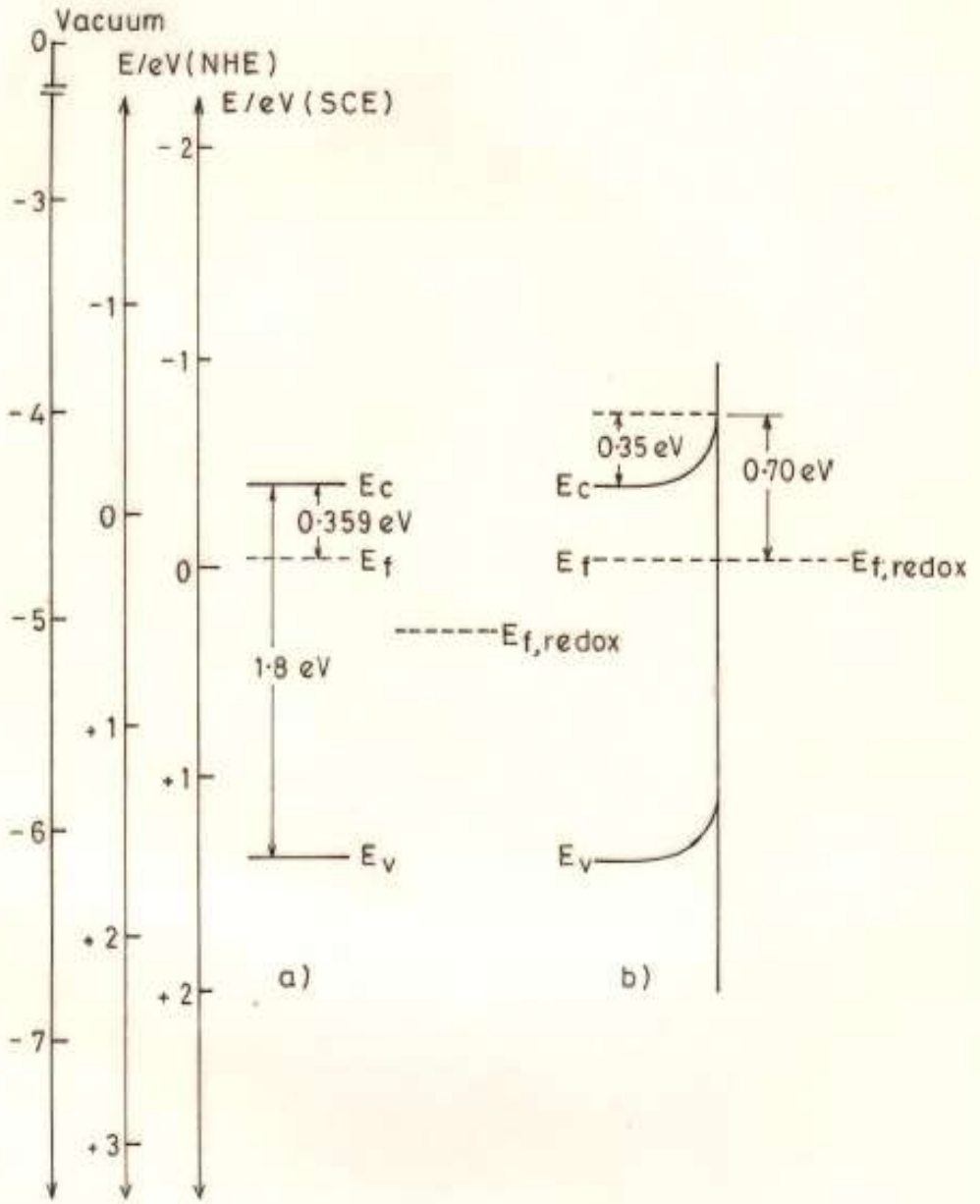

Fig. 7.22 a) n-Sb_2S_3/ polyiodide band diagram at flat-band condition.
b) Band bending at n-Sb_2S_3 (on Ti)/I^{3-}/I^- interface.

$$V_{bb} = V_{f,redox} - V_{fb} \quad (7.21)$$

$$= + 0.30 - (- 0.050)$$

$$= + 0.35 \text{ V}.$$

The barrier height V_B is calculated using

$$V_B = qeV_{bb} + (E_C - E_F) \quad (7.22)$$

and it comes out to be 0.709 V. The band bending diagram is obtained using the calculated values of various parameters and is shown in Fig. 7.22 (b). Based on these parameters, the width of depletion layer is calculated by the relation

$$W = (2 \varepsilon_O \varepsilon_S V_{bb} / e N_D)^{1/2} \quad (7.23)$$

Summary of results obtained from Mott-Schottky plots for Sb_2S_3 film on various substrates is given in Table 2.

The difference in observed location of the bands and the various values for the films deposited on three different substrates is due to the difference in grain size and defect density; as the films were prepared at two different temperatures, of the films. As we go from Ti to FTO substrates W go on increasing which reflects the increase in grain size and concurrent decrease in the scattering by grain boundaries. Relatively less R_s and higher ff for the films prepared on FTO coated substrates also supports these results.

Table 2 : Summary of results obtained from Mott- Schottky plots of *n*- Sb_2S_3/ polyiodide/ C PEC cell.

Sr. No.	Physical parameter	Value obtained on		
		Ti	S.S.	FTO
1.	Electrolyte used	I^{3-}/I^{-}	I^{3-}/I^{-}	I^{3-}/I^{-}
2.	$E_{f,redox}$ (eV_{SCE})	0.307	0.307	0.307
3.	V_{fb} (eV_{SCE})	– 0.050	– 0.115	– 0.260
4.	Donor concentration, N_D (cm^{-3})	1.095×10^{12}	4.81×10^{10}	2.12×10^{10}
5.	Density of states in conduction band, N_C, (cm^{-3})	1.17×10^{18}	1.17×10^{18}	1.17×10^{18}
6.	$E - E_F$ (eV_{SCE})	0.359	0.440	0.461
7.	Band bending V_{bb} (eV_{SCE})	0.350	0.415	0.560
8.	Barrier height, V_B	0.709	0.855	1.0221
9.	Depletion width, W (μm)	0.079	0.414	0.724
10.	Conduction band edge, E_C (eV_{SCE})	– 0.40	– 0.58	– 0.82
11.	Valence band edge, E_V (eV_{SCE})	1.40	1.22	0.98
12.	Carrier type	*n*	*n*	*n*

REFERENCES

1. S. Licht, Interface, The Electrochemical Society, "Fall"- issue, 1997 (p.34).

2. C.D. Lokhande, Solar Cells, 22 (1987) 133.

3. A. Aruchamy, G. Aravamudan and G.V. Subba Rao, Bull. Mater. Sci., 4 (1982) 483.

4. S. Chandra and R.K. Pandey, phys. stat. sol. (a), 72 (1982) 415.

5. V.D. Das and L. Damodare, Mater. Chem. Phys., 56 (1998)116.

6. O. Savadogo and K.C. Mandal , J. Electrochem. Soc. , 139 (1992) L16.

7. L.P. Deshmukh , M.I. Belle, B.M. More and P.P. Hankare, Bull. of Electrochem., 9 (1993) 245.

8. J.D. Desai and C.D. Lokhande , Bull. of Electrochem., 9 (1993) 242.

9. L.P. Deshmukh , S.G. Holikatti, B.P. Rane , M.I. Belle and P.P. Hankare, Bull. of Electrochem, 9 (1993) 237.

10. L.P. Deshmukh , S.G. Holikatti, B.P. Rane , B.M. More and P.P. Hankare , J. Electrochem. Soc., 141 (1994) 1779.

11. V.V. Killedar , C.D. Lokhande , C.H. Bhosale , Ind. J. Pure and Appl. Phys., 36 (1998) 33.

12. V.D. Das and L. Damodare, J. Appl. Phys., 81 (1997) 1522.

13. R. Krishnakumar, V. Subramanian, Y. Ramprakash and A.S. Lakshmanan, Mater. Chem. Phys., 15 (1987) 385.

14. J. B. Mooney and S. B. Radding, Ann. Rev. Mater. Sci., 12 (1982) 81.

15. Pramod S. Patil, Mater. Chem. Phys., 1999 (In Press).

16. V.V. Killedar , C.D. Lokhande and C.H. Bhosale , Mater. Chem. Phys., 47 (1997) 104.

17. K.Y. Rajpure, C.D. Lokhande and C.H. Bhosale, J. Phys. Chem. Solids, 1999 (Revised Submitted).

18. L.P. Deshmukh, V.S. Sawant and P.P. Hankare, Solar Cells, 31 (1991) 557.

19. M.D. Uplane and S.H. Pawar, Solar Cells, 10 (1983) 177.

20. L.P. Deshmukh , A.B. Palve and V.S. Sawant, Sol. Energy Mater., 20 (1990) 341.

21. S. Chandra in Photoelectrochemical Solar Cells, Gorden and Breach Science Publishers, New York (1985).

22. T.J. Coutts, Sol. Energy Mater., 50 (1978) 99.

23. R. Tenne and N. Muller, J. Electrochem. Soc., 130 (1983) 852.

24. J. D. Desai and C.D. Lokhande, Trans. of SAEST, 24 (1994) 111.

25. P.S. Patil, C.D. Lokhande and S.H. Pawar, J. Phys. D : Appl. Phys., 22 (1989) 550.

26. M.A. Butler, J. Appl. Phys., 48 (1977)1914.

27. J. I. Pankov, Optical Processes in Semiconductors, N. Holonyak Jr.(Ed.) (NJ : Solid State Physical Electronic Series, Prentise Hall, Englewood Clifls) 1971 (p.34).

28. Y. Ramprakash, V. Subramanian, R. Krishnakumar, A. S. Lakshmanan and V. K. Venkatsen , J. Power Source, 24 (1988) 329.

29. N.F. Mott, Proc. R. Soc., A171 (1939) 27.

30. W. Schottky, Z. Phys., 113 (1939) 367.

31. I.P. Grigas, V.F. Kunigelis, A.S. Orlyukas and V.I. Samulionis, Sov. Phys. - Solid State, 14 (1972) 796.

32. V.D. Das and L. Damodare, Mater. Chem. Phys., 56 (1998)48.

33. P. Herrasti, E. Fatas, J. Herrero and J. Ortega, Electrochim. Acta, 35 (1990) 345.

34. W.H. Laflere, F. Cardon and W.P. Gomes, Surf. Sci., 44 (1974) 541.

35. R. Memming, J. Electrochem. Soc., 116 (1969) 785.